ACS APPLIED MATERIALS & INTERFACES

Research Article

www.acsami.org

Construction of Highly Ordered ZnO–TiO_2 Nanotube Arrays (ZnO/TNTs) Heterostructure for Photocatalytic Application

Fang-Xing Xiao*

State Key Laboratory Breeding Base of Photocatalysis and College of Chemistry and Chemical Engineering, Fuzhou University, Fuzhou, 350002, P. R. China

Supporting Information

ABSTRACT: In recent years, strenuous efforts have been devoted to exploring ZnO functionalized TiO_2 nanotube arrays (ZnO/TNTs) nanocomposites; however, there is still a paucity of reports on the construction of well-defined ZnO/TNTs heterostructure via efficient and easily accessible approach. In this work, drawing on a two-step anodization combined pyrolysis strategy, we attained a highly ordered ZnO/TNTs hybrid nanostructure. Combined with a collection of characterizations including X-ray photoelectron spectroscopy (XPS), X-ray diffraction (XRD), diffusion reflectance spectrum (DRS), scanning electron microscopy (SEM), and transmission electron microscopy (TEM), we found that, in this coupling, in situ formed ZnO phases were uniformly grafted to TNTs framework giving rise to hybrid nanostructure, which is ascribed to cooperative interfacial interaction between polar TiO_2 layer and ZnO precursor. The underlying interaction leading to judicious combination of TNTs and ZnO was unveiled by Fourier transformed infrared spectrum (FTIR) and XPS. Alternatively, it has been shown that ZnO nanocrystals distributed on the TNTs could serve as favorable hole channels and receptors for efficient separation of photoexcited charge carriers, which results in significantly enhanced photocatalytic performances of ZnO/TNTs heterostructure in comparison with pure TNTs, ZnO film, and P25 particulate film. Furthermore, it is found that the hybrid photocatalyst demonstrated excellent photostability. It is hoped that our work could present a straightforward paradigm for preparation of hierarchical semiconductor/1-D semiconductor heterostructures.

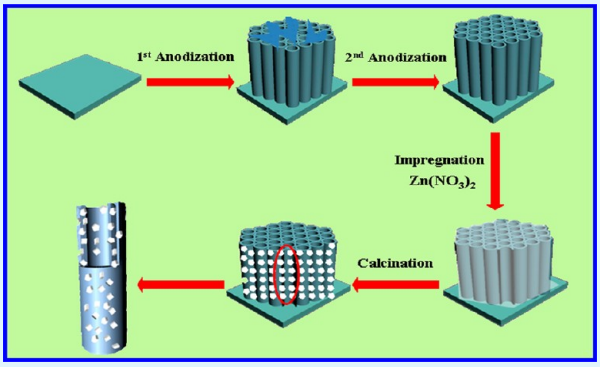

KEYWORDS: *ZnO, TiO_2 nanotube arrays, photocatalysis, heterostructure*

1. INTRODUCTION

One-dimensional (1-D) nanostructured semiconductoring materials, such as nanorodes, nanowires, and nanotubes have garnered considerable attention because of their unique physical and chemical properties, as well as their use in a myriad of fields,[1−3] especially for heterogeneous photocatalysis.[4−6] Among copious 1-D inorganic nanostructures, titania (TiO_2) nanotube to date has been extensively pursued as quintessential photocatalyst, for example, degradation of pollutants in air or water, and H_2 generation,[7,8] by virtue of high surface-to-volume ratio and superior physicochemical properties.[9] Moreover, nanotubular TiO_2 has been evidenced to manifest intrinsic advantages over counterparts of TiO_2 nanoparticles in terms of shape-depedent structure and properties.[10,11] It is thus highly desirable to fabricate and design 1-D TiO_2-based nanostructures for promising heterogeneous photocatalysis.

Thus far, various chemical routes, such as anodized aluminum oxide (AAO) template-assisted sol−gel method,[12,13] electrodeposition method,[14] and hydrothermal treatment of fine TiO_2 particles with alkaline solution,[15] have been developed for fabricating TiO_2 nanotube. Nonetheless, these methods often confront problems of template removel, tedious operation procedures, and poor adhension of nanotube to the underlying substrate, etc. In contrast, anodization of Ti foil leading to vertically aligned TiO_2 nanotube arrays (TNTs), as an alternative strategy, has sparked burgeoning interest, which possesses virtues of simplicity and efficiency, and moreover, it represents a unique combination of highly functional features of TiO_2 with a regular and controllable nanoscale geometry.[16−18] Research efforts have therefore been prompted to unveil wide-ranging photocatalytic applications of TNTs-based nanostructures.[19−29] Besides, as another promising heterogeneous photocatalyst, ZnO is also an excellent n-type semiconductor exhibiting comparable efficiency for various photocatalytic reactions,[30−32] when compared with TiO_2.

A formidable challenge, nevertheless, still remains in reducing quick recombination rate of photogenerated electron−hole pairs of TiO_2 and ZnO. Although transformation of TiO_2 to nanotubular structure may open a convenient avenue for improving photocatalytic efficiency, it can not tackle the central issue of photocatalysis.[33] On the other hand, ZnO normally

Received: October 26, 2012
Accepted: November 27, 2012
Published: November 27, 2012

suffers from intrinsic drawback of photocorrosion, which greatly reduces its photoactivity and photostability.[7,34] As a result, it still posts a long-standing challenge to resolve these fundamental disadvantages for diverse aspects of photocatalytic applications.

To solve these problems, research activities have been proliferated to reinforce the photocatalytic properties by manipulating nanostructures or morphologies of TiO_2 and ZnO,[35,36] including polymer passivation,[37] surface doping with nonmetallic/metallic elements or semiconductor oxides,[38−44] and surface deposition of metal nanoparticles.[45−47] In these cases, of particular note is the nanosized coupling of TiO_2 and ZnO that has been well-established to remarkably enhance the separation efficiency of photoexcited charge carriers because of the formation of heterojunction structure between them,[48,49] thus boosting quantum efficiency and photostability of the hybrid photocatalyst. Although the binding energies of ZnO and TiO_2 are analogous to each other,[50,51] notably, potentials of the conduction band and the valence band of ZnO are still charged a bit more negative than those of TiO_2. It is, accordingly, speculated that lower band gap energy may be attained when TiO_2 and ZnO were ingeniously combined in an appropriate way.[32] Currently, research interests have centered around design and synthesis of the ZnO/TiO_2 nanocomposites, such as ZnO−TiO_2 composite nanoparticles,[48,49] nanofilms,[52−54] and many other hybrid nanostructures,[55,56] of which coupled photocatalysts consisting of nanocrystalline TiO_2 and nanosized ZnO exhibit significantly enhanced photocatalytic activity resulting from synergic effect, as compared with single metal oxide. Inspired by this, combined with structural advantages of TNTs as starting nanobuilding blocks, highly ordered ZnO/TNTs hybrid nanostructure with promising photocatalytic efficiency can be expected.

More recently, chemical, electrochemical, and physical approaches have been developed to fabricate the ZnO/TNTs nanomaterials, such as template-assisted strategy,[57−59] hydrothermal method,[60,61] electrodeposition approach,[62] and filtered cathodic-vacuum-arc technique.[63] Despite the endeavors, protocols developed by these strategies are time-consuming and complicated. Moreover, TNTs used in these papers are jointly fabricated via conventional one-step anodization approach and inevitably featured by rough top surface and poor alignment, therefore resulting in weak interfacial contact between TNTs and ZnO.[64] In this regard, two-step anodization of Ti foil, as an efficient and economical approach, has been harnessed to improve the uniformity and orderliness of the TNTs.[65] Furthermore, it is revealed that photocatalytic properties of the ZnO/TNTs heterostructure in previous work were tentatively explored and have yet to be specifically elucidated. On the other hand, uniform distribution of ZnO nanocrystal on the scaffold of TNTs is seldomly reported due in large part to weak interfacial contact reaped via synthetic approaches as aforementioned above. Hence, judicious combination of ZnO and TNTs leading to well-defined hybrid heterostructure as efficient photocatalyst is highly desired.

Herein, we harness a facile two-step anodization combined pyrolysis route to construct 1-D highly ordered ZnO/TNTs heterostructure, by which in situ formed ZnO nanocrystals were evenly grafted on the TNTs framework. The crystal phases, morphologies, optical properties, and photocatalytic performances of the ZnO/TNTs heterostructures were explored to clarify the structure−property correlation. The active species in the photodegradation process are determined. Moreover, underlying mechanism responsible for well-defined morphology of the ZnO/TNTs heterostructure was tentatively probed. The ensemble of results shows that enhanced separation of electron−hole pairs and excellent photostability of the ZnO/TNTs heterostructure have been attained, owing to the formation of heterojunction structure which intimately combines ZnO with TNTs. It is envisioned that our work may provide new insights for preparation of semiconductor/1-D semiconductor hybrid nanostructures.

2. EXPERIMENTAL SECTION

2.1. Materials. The following materials were used: titanium sheets (50 mm ×20 mm ×0.1 mm, 99.9%, Xin RuiGe. Co. Beijing), deionized water (ddH_2O, Milipore, 18.2 MΩ·cm resistivity), zinic nitrate [$Zn(NO_3)_2$], graphite sheet (50 mm ×20 mm ×0.1 mm, 99.6%, Xin RuiGe. Co. Beijing), ethylene glycol ($(CH_2OH)_2$, ammonium fluoride (NH_4F), hydrogen fluoride (HF), nitric acid (HNO_3), hydrochloric acid (HCl). All of the materials were analytical grade and used as received without further purification.

2.2. Preparation of TNTs via Two-Step Anodization Approach. Highly ordered TNTs were fabricated by anodizing Ti foil in a two-electrode electrochemical cell. Briefly, the anodization was carried out by using Ti foil as a working electrode and graphite sheet as a counter electrode at room temperature (25 °C). Before anodization, Ti foils were first degreased with acetone and ethanol for 15 min by ultrasonication, respectively, rinsed with ddH_2O in turn, and dried in air. In the first-step anodization (1st anodization), the cleaned Ti foil was anodized in a 200 mL of ethylene glycol solution containing 0.3 wt % NH_4F and 2 vol % H_2O at 40 V for 10 h, and the nanotube layer was grown on the foil surface. The resultant nanotube layer was removed by ultrasonication in ddH_2O for 30 s, and a mirror surface of Ti was thus exposed. A second-step anodization (2nd anodization) was subsequently carried out under the same conditions for 2 h to produce well-aligned framework of TNTs. The thus-obtained samples were cleaned with ddH_2O, dried off with N_2 gas, and annealed at 450 °C for 3 h in air to transform the amorphous phase of TNTs to the crystalline anatase form. Finally, the TNTs were carefully ultrasonicated for 5 s to remove the irregular top layer of mesopores.

2.3. Preparation of the ZnO/TNTs Heterostructures. ZnO were deposited in TNTs by a one-step pyrolysis approach. Specifically, a designated amount (0.92 g, 1.84 g, 2.76 g, and 3.68 g) of $Zn(NO_3)_2$ was added to 20 mL of ethanol aqueous solution (i.e., 8 mL of ethanol plus 12 mL of ddH_2O), and pH was controlled to be ∼ 8. Then TNTs were immersed in the above mixed solutions for 4 h. Subsequently, the pretreated samples were annealed at 400 °C for 2 h in air with heating rate of 2 °C/min to transform absorbed precursor to ZnO phase, leading to ZnO/TNTs heterostructures with varied weight loading percentage of 5%, 10%, 15%, and 20%, respectively. *It should be emphasized that loading percentage herein is defined as weight ratio of $Zn(NO_3)_2$ to weight for mixed ethanol aqueous solution.* Meanwhile, P25 particulate film was fabricated for comparison. P25 (Degussa, 80: 20% anatase-rutile) particulate film was deposited on a Ti foil by a doctor-blade method using a slurry of 20 wt % P25 TiO_2 in ethanol; The thickness of P25 particulate film was examined by cross-sectional images of SEM image to control the same thickness to that of TNTs (6 μm) and ZnO/TNTs (15%) by loading adequate amount of P25-ethanol slurry and was also reinforced by annealing at 450 °C in air for 3 h.[66−69] The preparation of ZnO film was achieved by immersing glass slide precleaned with ethanol and ddH_2O in $Zn(NO_3)_2$ ethanol aqueous solution for 4 h, followed by annealing at 400 °C for 2 h, the same experimental conditions to that of ZnO/TNTs heterostructures. The thickness of pure ZnO film was mediated by tuning appropriate $Zn(NO_3)_2$ amount and its thickness was also examined by cross-sectional images of SEM image to guarantee the same thickness to that of ZnO/TNT (15%).

2.4. Characterization. The phase composition of the samples was determined by XRD on a Bruker D8 Advance X-ray diffractometer with Cu Kα radiation. The accelerating voltage and applied current were 40 kV and 40 mA, respectively. TEM, energy-dispersive X-ray

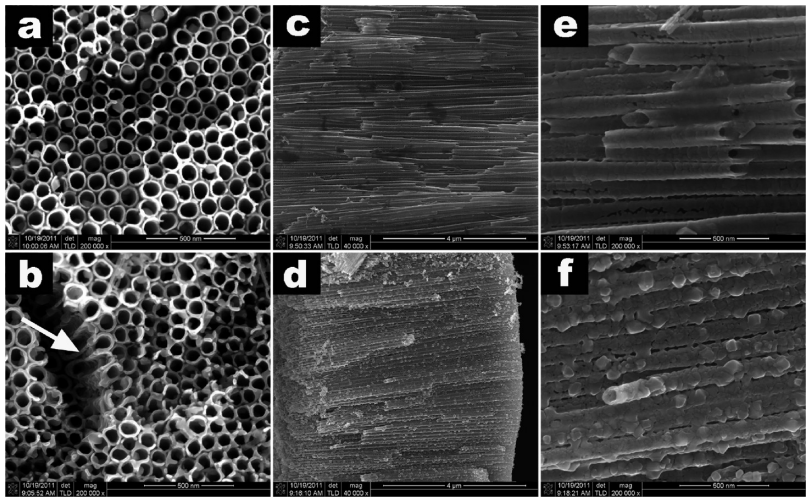

Figure 1. Panoramic views of (a) TNTs fabricated via two-step anodization approach and the as-prepared (b) ZnO/TNTs heterostructure, cross-sectional images of (c and e) TNTs, and (d and f) ZnO/TNTs heterostructure (15%). Panels e and f correspond to the magnified images in panels c and d, respectively.

spectrometer (EDX), and high-resolution TEM (HRTEM) images were obtained by a JEOL model JEM 2010 EX instrument at a accelerating voltage of 200 kV. The UV−vis DRS were recorded on a Varian Cary 500 Scan UV−vis−NIR spectrometer, in which $BaSO_4$ was used as the background between 200 and 800 nm scope. XPS measurement was conducted on an ESCALAB 250 photoelectron spectrometer (Thermo Fisher Scientific) at 2.4×10^{-10} mbar using a monochromatic Al $K\alpha$ X-ray beam (1486.60 eV). All the binding energies of the elements were calibrated to carbon binding energy of 284.60 eV which corresponds to standard hydrocarbon energy of C−H and C−C bonds. The morphology of the sample was characterized by field emission SEM (FESEM/EDX, FEI Nova NanoSEM 230). FTIR spectra were recorded in the transmittance mode with a resolution of 4 cm^{-1} using a Nicolet Nexus 670 FTIR spectrometer.

2.5. Photocatalytic Activity. Photocatalytic activity was evaluated by using Rhodamine B (RhB) as a model organic dye pollutant compound. In a typical test, samples with the same area of 30 mm ×10 mm were soaked into 3.0 mL of RhB aqueous solution (5 mg/L) at pH value of 7 in a quartz cuvette. Before irradiation, the mixtures were kept in the dark for 1 h to reach equilibrium of adsorption−desorption at room temperature. A 300 W Xe arc lamp (PLS-SXE 300C) equipped with a cutoff filter (λ = 365 ± 15 nm) was applied as UV light source. A commercial electric fan was used to cool the reaction system. The irradiation time ranged from 30 min to 2.5 h. Under ambient conditions, all the samples in the quartz cuvette were placed 15 cm away from the UV source. At each irradiation interval of 30 min, light absorption of the reaction solution was measured by a Cary 500 scan UV−vis spectrophotometer. The concentration of RhB was determined by the absorption of RhB at 553 nm. The degradation ratio of RhB at each time interval was calculated from the ratio of the light absorbance of irradiated to the nonirradiated solution.

2.6. Photoelectrochemical Measurement. Photoelectrochemical measurement was performed on a CHI 600D electrochemical system (Chenhua Instruments, Co., Shanghai). The testing system was comprised of three electrodes, a single-compartment quartz cell, which was filled with 0.1 M Na_2SO_4 electrolyte (30 mL), and a potentiostat. A platinum black sheet was used as a counter electrode with $Hg/Hg_2Cl_2/KCl$ as a reference electrode. A thin film of TNTs or ZnO/TNTs heterostructures with the same area of 3 cm^2 was employed as a working electrode. A 300 W Xe arc lamp (PLS-SXE 300C) equipped with a band-pass light filter (λ = 365 ± 15 nm) was used as the exciting light source for UV light irradiation.

3. RESULTS AND DISCUSSION

3.1. Preparation of the Well-Defined ZnO/TNTs Heterostructure. The morphologies of TNTs and ZnO/TNTs hybrid nanostructure were examined by field-emission SEM. From the FESEM images (Figure 1a, c, and e), it can be observed that TNTs framework prepared via two-step anodization approach exhibit well-aligned nanotubular structure which grows vertically from the Ti foil (Supporting Information Figure S1b), and the nanotubes are uniform manifesting an average pore diameter of ∼76 nm with rather smooth surface (Figure 1e). When the TNTs have gone through pyrolysis treatment, morphology of the hybrid nanostructure is distinctly different from that for blank TNTs, in which close packed quasi-square ZnO nanocrystals with mean diameter of around 50 nm were uniformly distributed on the framework of TiO_2 nanotubes (Figure 1d and Figure 1f). Moreover, significantly, the in situ produced ZnO phases were intimately embedded in the whole cross-sectional profile of TNTs (Figure 1d), and no agglomeration of ZnO phases were observed. The more detailed information regarding structural features of the ZnO/TNTs heterostructure can refer to images displayed in Supporting Information Figure S1. The hierarchical morphology of the hybrid nanostructure may allude to cooperative interfacial interaction between TNTs scaffold and ZnO nanocrystals, which will be addressed in the later part.

Figure 2 portrays TEM images of blank TNTs and ZnO/TNTs heterostructure. As displayed in Figure 2a, TiO_2 nanotube is featured by hollow-core construction which agrees with SEM result. When combined with ZnO phase in situ prepared via two-step anodization combined pyrolysis technique, single TiO_2 nanotube separated was tightly wrapped by the ZnO nanocrystals (Figure 2b and c). The inset model in Figure 2b vividly depicts the hybrid nanostructures of ZnO/TNTs. The more specific images of Figure 2b are provided in Supporting Information Figure S2. High-resolution (HR) TEM image was taken at the boundaries between TNTs and ZnO building blocks. Clear and identical crystallographic orientations can be found on either side of the TiO_2 and ZnO border in both regions, in which lattice fringes of 0.352 and 0.260 nm in Figure 2c concur well with interplanar spacing of (101) and (002) crystallographic planes of TiO_2 and ZnO, respectively.

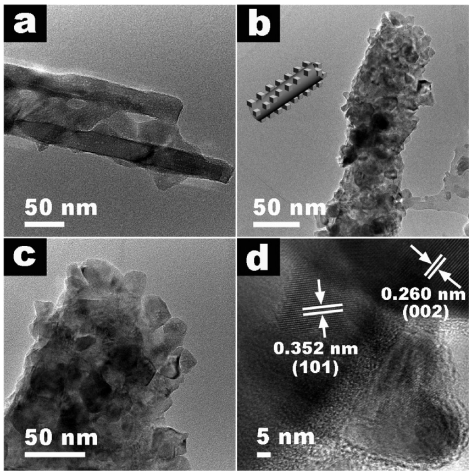

Figure 2. TEM images of (a) TNTs, (b–c) ZnO/TNTs with inset model, and (d) HRTEM images of the ZnO/TNTs heterostructure (15%).

Notably, a distinct boundary is visible and no transitional layer is found (Figure 2c) which indicates that ZnO nanocrystals were intimately distributed on the TiO_2 nanotubes to constitute a single composite nanotube in the fabrication process. Composition elements of the ZnO/TNTs heterostructure were demonstrated in the EDS pattern (Supporting Information Figure S2b), consisting of Ti, Zn, and O from bulk hybrid nanocomposites. The detection of C and Cu is originated from carbon-coated copper grid used for the TEM measurement. Thus, TEM result further discloses that two-step anodization combined pyrolysis approach developed in our work is beneficial for creating ZnO/TNTs hybrid heterostructure, in which second phase of ZnO nanocrystals were grafted to the framework of TNTs. The information on specific texture of the second phase was revealed by the XRD and XPS measurements.

Crystal structure of the samples was determined by XRD, as shown in Figure 3. The peaks (Figure 3a–b) at 2θ values of

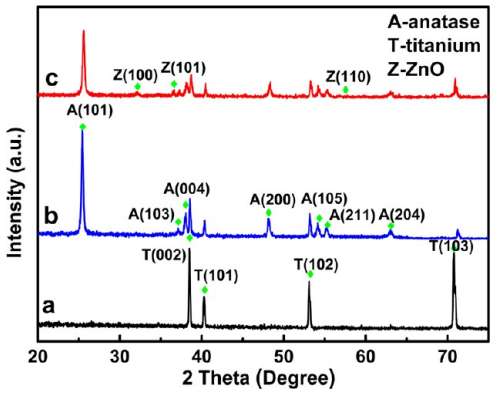

Figure 3. XRD patterns of TNTs (a) before and (b) after calcination at 450 °C in air for 3 h and (c) the ZnO/TNTs heterostructure.

25.3°, 37.8°, 48.0°, 53.9°, 62.7°, and 75.0° are undisputedly indexed to (101), (004), (200), (105), (204), and (215) crystal planes of anatase TiO_2 (JCPDF no. 21-1272), respectively. The peaks (Figure 3a–c) at 2θ values of 38.4°, 40.3°, 53.1°, and 70.8 ° match with (002), (101), (102), and (103) crystal planes of metal Ti phase (JCPDF no. 44–1294) from Ti foil. The peaks of anatase TiO_2 and Ti matrix are marked with A and T in Figure 3, respectively. Combined with SEM and TEM results, Figure 3a and b reflect that calcination treatment of TNTs at 450 °C in air for 3 h does not modify the highly ordered morphology of TNTs, but rather transform the TNTs from the amorphous phase to the anatase phase. It should be emphasized that such post-treatment of TNTs is essential to trigger significantly enhanced photocatalytic performances of TNTs and ZnO/TNTs, since anatase TiO_2 has been evidenced to be more effective in most of the studied cases.[46,47] Crystal phase of the ZnO/TNTs heterostructure is displayed in Figure 3c, in which anatase TiO_2 and hexagonal wurtzite-type ZnO (JCPDF no. 36-1451) form the dominant phases. The sharp and intense diffraction peaks suggest a high crystallinity of the samples.

To further uncover the composition of the samples, XPS was employed to probe surface property of the ZnO/TNTs hybrid nanocomposite. Gaussian deconvolution of the high-resolution spectra was applied to differentiate varied chemical bond species, and particularly, elemental chemical states in the samples. As shown in Figure 4a, ZnO/TNTs hybrid

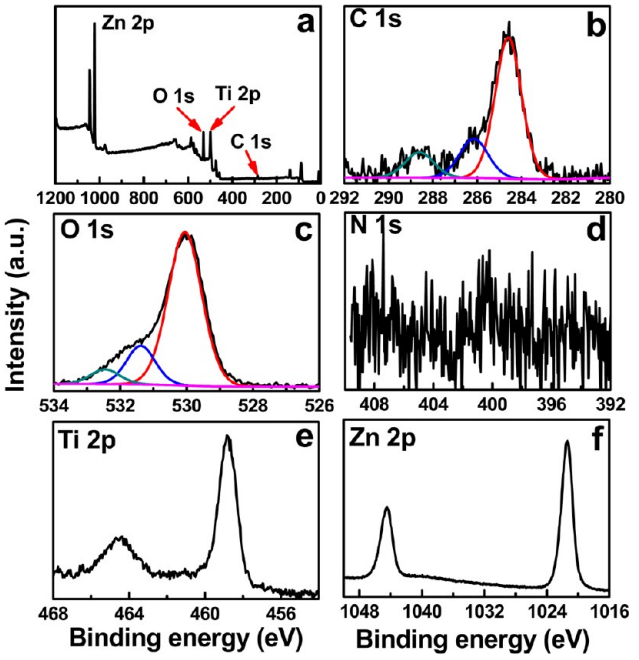

Figure 4. (a) Survey and high-resolution XPS spectra of (b) C 1s, (c) O 1s, (d) N 1s, (e) Ti 2p, and (f) Zn 2p for the ZnO/TNTs heterostructure.

nanostructure is mainly composed of four elements, that is, C 1s, O 1s, Ti 2p, and Zn 2p. For C 1s spectrum, the major peak at 284.60 eV is attributed to surface C–C or C–H bonds,[70–72] and the second peak 286.15 eV is attributed to carbon atoms presented in surface C–OH or C–O–C groups.[73,74] The third peak at 288.61 eV is assigned to surface –COO-group.[71] As for O 1s spectrum, the first peak at 530.05 eV is attributable to lattice oxygen in the TiO_2 and ZnO (i.e., Ti–O and Zn–O).[75] The second peak at 531.38 eV is assigned to the oxygen in surface hydroxyl groups for TiO_2 and ZnO (i.e., Ti–OH and Zn–OH),[76] and the third peak at 532.46 eV is assigned to the oxygen in C–OH/C–O–C corresponding to the C 1s specie at 286.15 eV.[77] Noticeably, no N 1s signal was observed in the ZnO/TNTs heterostructure, which corroborates successful

pyrolysis of $Zn(NO_3)_2$ after heat treatment giving rise to pure ZnO phase (Figure 4d). As shown in Figure 4e, featured peaks with binding energy (BE) of 458.84 eV (Ti $2p_{3/2}$) and 464.41 eV (Ti $2p_{1/2}$) in core-level spectrum of Ti agree with anatase TiO_2 (Ti^{4+}).[78,79] This indicates distribution of ZnO phase on the framework of TNTs did not modify texture property of TiO_2 substrate. High-resolution spectrum of Zn 2p (Figure 4f) displayed characteristic peaks of 1021.38 eV (Zn $2p_{3/2}$) and 1044.47 eV (Zn $2p_{1/2}$) corresponding to chemical element state of Zn^{2+} (ZnO).[80,81] The detailed chemical bond species versus BE is listed in Supporting Information Table S1. Consequently, XPS analysis determines property of the ZnO/TNTs heterostructure which is made up of anatase TiO_2 of TNTs and ZnO, and it manifest faithful agreement with XRD result.

UV−vis DRS are utilized to determine the optical properties of the samples. Figure 5 shows that both TNTs and ZnO/TNTs hybrid nanostructure exhibit a pronounced adsorption band in the region spanning from 200 to 400 nm, which is ascribed to electron promotion from the valence band to the conduction band.[9] It should be noted that adsorption peak of ZnO at 360 nm is almost shield by that for bulk TiO_2 nanotube in the UV-light regime. Moreover, DRS of ZnO/TNTs heterostructures with varied impregnated percentage of precursor were also demonstrated in Supporting Information Figure S3, which reflects analogous absorbed band edge, indicating photosensitivity of the hybrid nanostructures is independent of the weight loading amount of precursor. Accordingly, DRS result mirrors substantial UV light photosensitivity of TNTs and ZnO/TNTs heterostructures for photocatalytic applications.

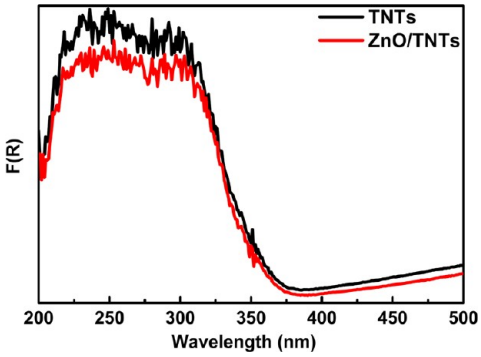

Figure 5. UV−vis diffuse reflectance spectra (DRS) of TNTs and ZnO/TNTs heterostructure.

To recapitulate, combinatorial techniques of SEM, TEM, XRD, XPS, and DRS indicate successful preparation of well-defined ZnO/TNTs heterostructures via two-step anodization combined one-step pyrolysis approach, by which in situ formed quasi-square ZnO nanocrystals were uniformly grafted to the framework of TNTs based on intimate interfacial contact between ZnO or $[Zn(NO_3)_2]$ and hydrophilic surface of TiO_2 nanotube. The underlying mechanism regarding the formation of ZnO/TNTs hybrid nanostructures will be highlighted in the following part.

Figure 6 depicts fabrication process of the well-defined ZnO/TNTs heterostructure via the two-step anodization combined pyrolysis approach. The frameworks of TiO_2 nanotube arrays used in our work were fabricated via two-step anodization (2nd anodization) approach, by which disordered surface layer inherited from conventional one-step anodization (1st anodization) technique were completely removed, therby leading to highly ordered nanotube arrays.[47] Noteworthily, TiO_2 nanotube fabricated *via* direct first anodization is detrimental to uniform impregnation of $Zn(NO_3)_2$ by virtue of its rough top surface and poor alignment (the first step in Figure 6). Therefore, ZnO/TNTs heterostructure was prepared by two-step anodization combined pyrolysis technique in which ZnO phases resulting from pyrolysis of $Zn(NO_3)_2$ were directly dispersed in the framework of TNTs. As well, it is found that TNTs was closely wrapped by monodisperse ZnO from local enlarged image (circles marked in Figure 6 and Supporting Information Figure S1).

The formation of hierarchical ZnO/TNTs heterostructure may be attributed to three reasons. First, superhydrophilicity of the TiO_2 surface is highly advantageous for absorbing polar aqueous precursor to make $Zn(NO_3)_2$ completely impregnated into interior and external surfaces of the TNTs, thus contributing to uniform distribution of ZnO nanocrystals. Secondary, negatively charged TiO_2 layer is beneficial for spontaneous absorption of Zn^{2+} on the TNTs surface via

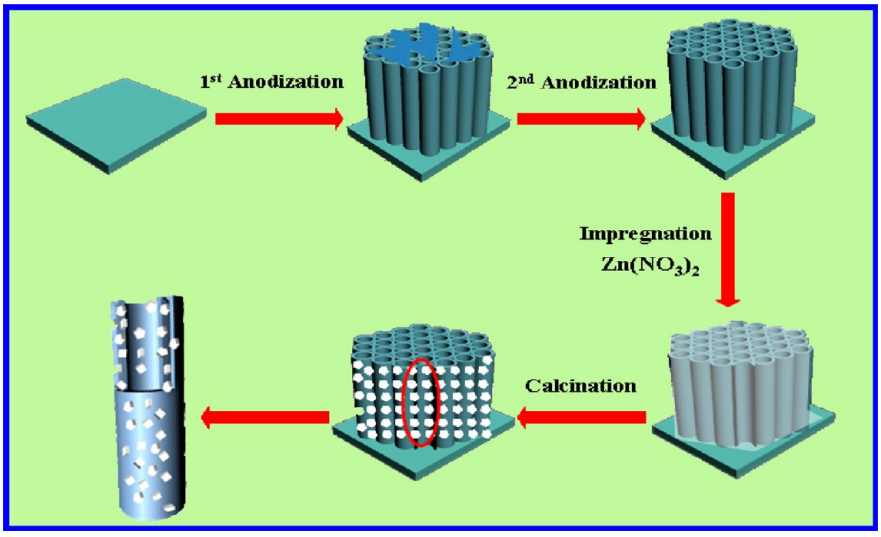

Figure 6. Flowchart illustrating the two-step anodization combined pyrolysis patterning of the hierarchical ZnO/TNTs heterostructure.

substantial electrostatic interaction force, owing to higher pH value of reaction system than isoelectric point (IEP) of TiO_2 (4.5–6.8).[82] Third, intimate interfacial interaction between ZnO and TiO_2 via chemical bonding is also speculated to be responsible for the well-defined morphology of the heterostructure, which can be revealed by XPS and FTIR results.

Figure 7 illustrates FTIR results of the ZnO/TNTs heterostructure and plain TNTs, in which featured peaks at

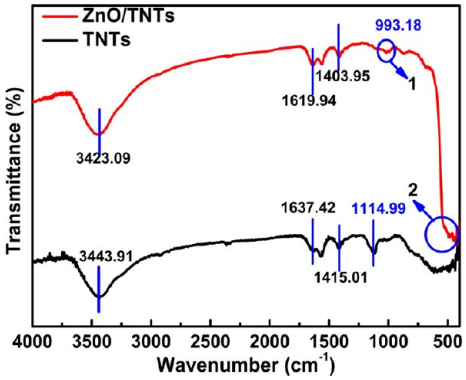

Figure 7. Fourier transformed infrared (FTIR) spectra of TNTs and ZnO/TNTs heterostructure.

3443.9, 1637.4, 1415.0, and 1115.0 cm^{-1}, correspond to fingerprint stretching vibration modes of surface OH and Ti–O asymmetric vibration,[83] respectively, for TNTs. Significantly, these characteristic peaks of TNTs blue-shift to 3423.1, 1612.0, 1404.0, and 993.2 cm^{-1}, respectively, after combining with ZnO nanocrystals. Particularly, intensity of the Ti–O peak (1114.99 cm^{-1}) in TNTs was greatly reduced (circle 1) accompanying with substantial wavenumber shift of 122 cm^{-1} (1114.99 vs 993.18 cm^{-1}), this evinces the Ti–O bonds of TNTs may be partly replaced by the Zn–O bonds for the formation of heterojuction structure and Zn–O–Ti linkage in the interface between ZnO and TiO_2. In addition, pronounced peak of 490 cm^{-1} corresponding to the Zn–O bond arised as compared with blank TNTs (circle 2),[45,84] indicating the replacement of Ti–O with Zn–O in the ZnO/TNTs heterostructure, which conforms to the above deduction.

Supporting Information Table S1 displays detailed chemcial bond species versus BE for the TNTs and ZnO/TNTs heterostructure. It is noted that lattice oxygen of TNTs (i.e., Ti–O) exhibits pronounced BE shift of 0.23 eV (529.82 vs 530.05 eV)[46] and moreover, Ti $2p_{3/2}$ and Ti $2p_{1/2}$ species of TNTs also demonstrated BE shitfs of 0.29 eV (458.55 vs 458.84 eV) and 0.16 eV (464.25 vs 464.41 eV),[46] which corroborates perturbation of Ti–O bonds in TNTs with the functionalization of ZnO. Based on the above analysis, it is speculated that the ZnO/TNTs heterostructures will demonstrate to be promising photocatalysts in view of their well-defined morphology and intimate interfacial contact between TNTs and ZnO.

3.2. Photocatalytic Performance of the ZnO/TNTs Hybrid Nanostructures. The photocatalytic performances of the TNTs and ZnO/TNTs heterostructure were evaluated by liquid-phase degradation of aqueous Rhodamine B (RhB), a model organic dye pollutant, under the irradiation of UV light (365 ± 15 nm). Blank experiments (i.e., without catalyst or UV light) evince negligible photocatalytic activities, thus corroborating the degradation reaction is truly driven by a photocatalytic process. It has been well-established that the photodegradation process of organic dye pollutant can be ascribed to a pseudofirst-order reaction which follows the simplified Langmuir–Hinshelwood model, that is, $\ln(C_0/C) = k_a t$, when C_0 is very small, where k_a is the apparent firs-order rate constant.[85] To highlight the advantage of ZnO/TNTs hybrid nanocomposites, pure ZnO and P25 particulate films with the same thickness were harnessed as reference counterparts. It is found that ZnO/TNTs heterostructure exhibits remarkably superior photocatalytic activity to its counterparts of P25 particulate film, pure ZnO film and plain TNTs, from the kinetic rate constant values (Figure 8a). The enhancement

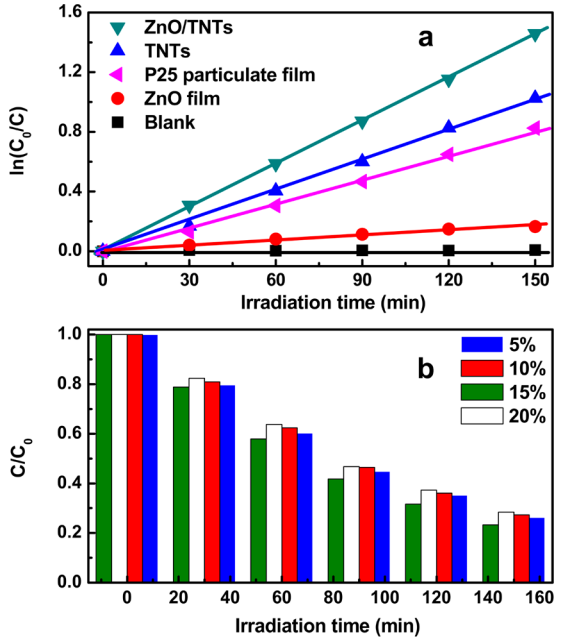

Figure 8. (a) Photocatalytic activities of TNTs, ZnO film, ZnO/TNTs heterostructure (15%), and P25 particulate film for photodegradation of RhB aqueous solution under ambient conditions. (b) Photocatalytic performance of the ZnO/TNTs heterostructure with varied deposition percentage of $Zn(NO_3)_2$ precursor in ethanol aqueous solution.

of the ZnO/TNTs hybrid nanostructures may arise from 2-fold cumulative contributions: on the one hand, self-aligned TNTs imparts multiple and long mean free path of charge carriers when compared with P25 or ZnO bulk material;[46] on the other hand, ZnO nanocrystals may increase surface area of the composite nanotube and maintain a large interfacial contact area to favor a heterojunction effect. Moreover, photocatalytic activities of the ZnO/TNTs heterostructures with different loading percentage of precursor were also tailored. As displayed in Figure 8b, ZnO/TNTs heterostructures with varied deposition amount of precursor exhibit no pronounced discrepancy in terms of photodegradation rate at ambient conditions, indicating there is a saturation value in our system for deposition of ZnO phase.

Figure 9 shows transient photocurrent responses of TNTs and ZnO/TNTs heterostructure over several on–off cycles of intermittent UV light irradiation (365 ± 15 nm). The anodic photocurrent spike produced by the UV light irradiation was observed with good reproducibility. It is well-known that photocurrent is originated from by the diffusion of the photogenerated electrons to the back contact and meanwhile the photoinduced holes are taken by the hole acceptor in the

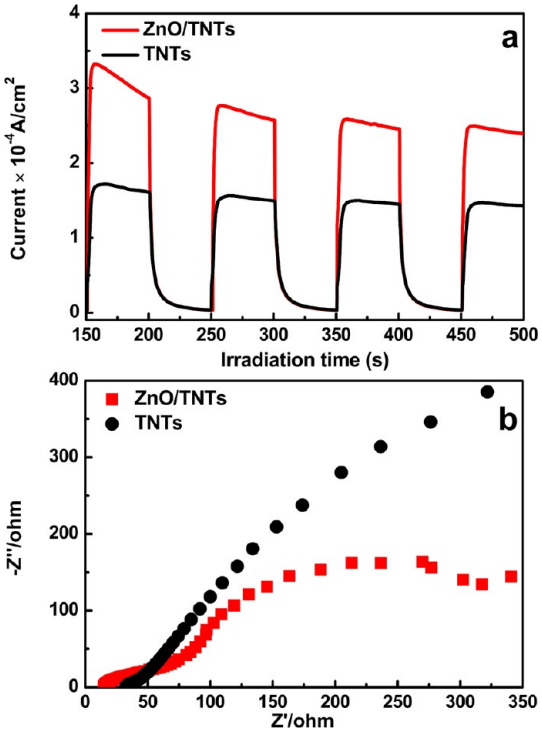

Figure 9. (a) Transient photocurrent responses and (b) electrochemical impedance spectroscopy (EIS) Nynquist plot of TNTs and ZnO/TNTs heterostructure (15%) in 0.1 M Na_2SO_4 aqueous solution without bias versus Pt counter electrode under UV light irradiation (365 ± 15 nm), the amplitude of the sinusoidal wave was set at 10 mV, and the frequency varied from 100 to 0.05 HZ.

electrolyte.[86] It is found that photocurrent response of the ZnO/TNTs heterostructure is nearly 2-fold higher than that of blank TNTs (Figure 9a), suggesting more efficient separation and longer lifetime of photoexcited electron−hole pairs of ZnO/TNTs as compared with TNTs. Besides, probably, Zn^{2+} of ZnO grafted on the TNT surface may act as surface-interface shallow traps and favor the suppression of photogenerated electron−hole pairs.[53] A sharp attenuation of the photocurrent was observed with the light off, indicating the recombination of photoexcited electrons and holes. On the other hand, EIS result (Figure 9b) reflects the impedance arc radius of the ZnO/TiO_2 heterostructure is smaller than that of TNTs, indicating ZnO/TiO_2 heterostructure demonstrates enhanced separation efficiency of photoexcited charge carriers when compared with TNTs. In this regard, transient photocurrent response and EIS results reveal analogous trend to the photocatalytic activities of the samples.

It has been well-established that ZnO generally suffers from photocorrosion for photocatalytic applications (Figure 10b),[87,88] hence it is of prime importance to probe the photostability of the ZnO/TNTs heterostructures. To this end, cyclic photodegradation experiments, XRD, and XPS were combined to access the evaluation. Figure 10a displays cycling experiments of the ZnO/TNTs hybrid nanostructure for photodegradation of RhB under irradiation of UV light (365 ± 15 nm). The result indicates that no noticeable change was observed even the photocatalyst went through four successive recycles, suggesting the ZnO/TNTs heterostructures are stable in chemical properties. Moreover, XRD patterns (Supporting Information Figure S4) of the used and fresh samples reveal intact crystalline phase of the ZnO/TNTs heterostructure.

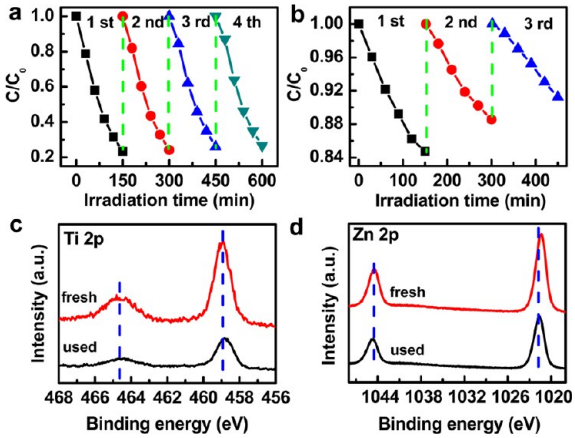

Figure 10. Cycling photodegradation of RhB aqueous solution over (a) ZnO/TNTs heterostructure (15%) and (b) pure ZnO film under ambiet conditions, high-resolution XPS spectra of (c) Ti 2p and (d) Zn 2p before and after recycled photocatalytic reactions over the ZnO/TNTs heterostructure (15%).

Furthtermore, high-resolution XPS spectra of Ti 2p (Figure 10c) and Zn 2p (Figure 10d) of the used sample exhibit no BE shift, both of which point to the same chemical element state of Ti^{4+} and Zn^{2+} to those of the fresh one, respectively. Consequently, XRD and XPS results further attest excellent photostability of the hybrid photocatalyst and photocorrosion of ZnO was significantly inhibited. Notably, such high efficiency and stability of the hybrid heterostructure have profound implication for practical applications in a slurry system, since no separation of photocatalyst is needed as a result of direct up-growth property of TNTs on the Ti foil, thereby boding well for inimitable advantages over its particulate counterparts.

3.3. Photocatalytic Mechanism Investigation. The principle of photocatalytic decomposition over ZnO/TNTs heterostructure is delineated in Figure 11. Although the band

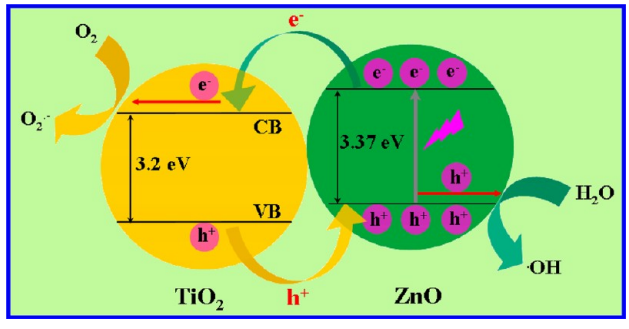

Figure 11. Schematic diagram illustrating the charge-transfer process in the ZnO/TNTs heterostructure when used as photocatalyst under UV light irradiation.

gap energies of ZnO and TiO_2 are similar to each other (around 3.37 vs 3.2 eV), nevertheless, potentials of the conduction band (CB) and the valence band (VB) of ZnO are still charged a bit more negative. When ZnO are irradiated by photon energy surpassing its band gap energy, electrons are photoexcited from the VB to the CB leaving holes in the VB, and then electrons transfer from the CB of ZnO to the CB of TiO_2 on accounts of potential difference between them, and conversely, holes transfer from the VB of TiO_2 to the VB of ZnO under UV excitation, leading to thermal equilibrium state

dx.doi.org/10.1021/am302462d | ACS Appl. Mater. Interfaces 2012, 4, 7055−7063

in this system (i.e., Fermi levels align).[87,89] More importantly, due to the presence of a ZnO−TNTs heterojunction (i.e., potential barrier), recombination of the photogenerated electron−hole charge carriers were markedly reduced. Additionally, electrons or holes that transfer to the TiO_2 or ZnO active surface of the hybrid nanostructures immediately join in the redox reactions, in which electrons reduce dissolved molecular oxygen to produce superoxide radical anions (O_2^-), while holes oxidize H_2O molecular to yield hydroxyl radicals (·OH). Organic dye pollutants (RhB) are eventually oxidized by these highly active species to CO_2 and H_2O products. The predominant active species in the ZnO/TNTs hybrid system were determind to be holes apart from hydroxyl radicals (Supporting Information Figure S5), which reveals the grafted ZnO could serve as favorable hole channels and receptors for efficient separation of photoexcited electrons and holes. Furthermore, nanotubular characteristic of TNTs and monodispersity of the ZnO may also contribute to reducing recombination of photoexcited electrons and holes owing to effective separation of space-charge,[46] both of which results in significantly enhanced photocatalytic performance of the hybrid nanostructures.

4. CONCLUSIONS

In summary, we have shown that three-dimensional arrayed ZnO/TNTs heterostructure can be fabricated *via* a facile two-step anodization combined pyrolysis approach, by which in situ formed ZnO nanocrystals were uniformly anchored in the framework of TNTs due to intimate interfacial contact between polar TiO_2 surface and ZnO precursor. The cooperative interaction between TNTs and ZnO in the ZnO/TNTs heterostructure was explored by FTIR and XPS. Moreover, the ZnO/TNTs heterostructure manifests superior photocatalytic activities to its counterparts of pure ZnO, TNTs, and P25 particulate film. The enhanced photocatalytic activities of the heterostructure can be primarily attributed to the large exposed surface area of TNTs to surrounding medium and formation of heterojunction structure in the interface between ZnO and TNTs which greatly promotes efficient separation of photogenerated electron−hole charge carriers. More significantly, the ZnO/TNTs hybrid system possesses excellent photostability and can be readily recovered owing to vertically growing properties of TiO_2 nanotube. Consequently, it is hoped that the two-step anodization combined pyrolysis patterning strategy in our work may open up a new avenue for exploring novel hierarchical photocatalysts for environmental remediation.

■ ASSOCIATED CONTENT

Ⓢ Supporting Information

Table for binding energy versus chemical bond species, additional SEM and TEM images for the ZnO/TNT heterstructure, DRS result for ZnO/TNT with different loading percentage of $Zn(NO_3)_2$, XRD pattern of ZnO/TNT before and after cycling photocatalytic reactions, and experiments for determination of the primary active species. This material is available free of charge via the Internet at http://pubs.acs.org.

■ AUTHOR INFORMATION

Corresponding Author

*E-mail: fangxing2010@gmail.com.

Notes

The authors declare no competing financial interest.

■ ACKNOWLEDGMENTS

The support by National Basic Research Program of China (973 Program: 2007CB613306) is greatly acknowledged.

■ REFERENCES

(1) Wang, Z. L. *Adv. Mater.* **2003**, *15*, 432−436.
(2) Kudo, A.; Miseki, Y. *Chem. Soc. Rev.* **2009**, *38*, 253−278.
(3) Tang, Z. R.; Zhang, Y. H.; Xu, Y.-J. *ACS Appl. Mater. Interfaces* **2012**, *4*, 1512−1520.
(4) Tada, H.; Mitsui, T.; Kiyonaga, T.; Akita, T.; Tanaka, K. J. *Nat. Mater.* **2006**, *10*, 782−786.
(5) Norris, D. J.; Efros, A. L.; Erwin, S. C. *Science* **2008**, *319*, 1776−1779.
(6) Zhang, N.; Zhang, Y. H.; Xu, Y.-J. *Nanoscale* **2012**, *4*, 5792−5813.
(7) Hoffmann, M. R.; Marin, S. T.; Choi, W.; Bahnemannt, D. W. *Chem. Rev.* **1995**, *95*, 69−96.
(8) Fox, M. A.; Dulay, M. T. *Chem. Rev.* **1993**, *93*, 341−357.
(9) Zhu, L.; Liu, G. C.; Duan, X. C.; Zhang, Z. J. *J. Mater. Res.* **2010**, *25*, 1278−1287.
(10) Jennings, J. R.; Ghicov, A.; Peter, L. M.; Schmuki, P.; Walker, A. B. *J. Am. Chem. Soc.* **2008**, *130*, 13364−13372.
(11) Tachikawa, T.; Majima, T. *J. Am. Chem. Soc.* **2009**, *131*, 8485−8495.
(12) Chu, S. Z.; Wada, K.; Inoue, S.; Todoroki, S. *Chem. Mater.* **2002**, *14*, 266−272.
(13) Miao, Z.; Xu, D.; Ouyang, J.; Guo, G.; Zhao, X.; Tang, Y. N. *Nano Lett.* **2002**, *2*, 717−720.
(14) Limmer, S. J.; Chou, T. P.; Cao, G. Z. *J. Mater. Sci.* **2004**, *39*, 895−901.
(15) Tian, Z. R.; Voigt, J. A.; Liu, J.; Mckenzie, B.; Xu, H. *J. Am. Chem. Soc.* **2003**, *125*, 12384−12385.
(16) Roy, P.; Berger, S.; Schmuki, P. *Angew. Chem., Int. Ed.* **2011**, *50*, 2904−2939.
(17) Wang, D. A.; Liu, L. F. *Chem. Mater.* **2010**, *22*, 6656−6664.
(18) Wang, D. A.; Liu, L. F.; Zhang, F. X.; Tao, K.; Pippel, E.; Domen, K. *Nano Lett.* **2011**, *11*, 3649−3655.
(19) Liu, S.; Yang, L.; Xu, S.; Luo, S.; Qai, Q. *Electrochem. Commun.* **2009**, *11*, 1748−1751.
(20) Ghicov, A.; Schmidt, B.; Kunze, J.; Schmuki, P. *Chem. Phys. Lett.* **2007**, *433*, 323−326.
(21) Mohapatra, S. K.; Misra, M.; Mahajan, V. K.; Raja, K. S. *J. Phys. Chem. C* **2007**, *111*, 8677−8685.
(22) Li, Q.; Shang, J. K. *Environ. Sci. Technol.* **2009**, *43*, 8923−8929.
(23) Lu, N.; Quan, X. J.; Li, Y.; Chen, S.; Yu, H. T.; Chen, G. H. *J. Phys. Chem. C* **2007**, *111*, 11836−11842.
(24) Furube, A.; Du, L. C.; Hara, K.; Katoh, R.; Tachiya, M. *J. Am. Chem. Soc.* **2007**, *129*, 14852−14853.
(25) Yang, L.; He, D.; Cai, Q.; Grimes, C. A. *J. Phys. Chem. C* **2007**, *111*, 8214−8217.
(26) He, B. L.; Dong, B.; Li, H. L. *Electrochem. Commun.* **2007**, *9*, 425−430.
(27) Milsom, E. V.; Novak, J.; Oyama, M.; Marken, F. *Electrochem. Commun.* **2007**, *9*, 436−442.
(28) Chen, X.; Zhang, X.; Su, Y.; Lei, L. *Appl. Surf. Sci.* **2008**, *254*, 6693−6696.
(29) Sun, L.; Li, J.; Wang, C.; Li, S.; Lai, Y.; Chen, H.; Lin, C. *J. Hazard. Mater.* **2009**, *171*, 1045−1050.
(30) Khodja, A. A.; Sehili, T.; Pilichowski, J. F.; Boule, P. *J. Photochem. Photobiol., A* **2001**, *141*, 231−239.
(31) Lizama, C.; Freer, J.; Baeza, J.; Mansilla, H. D. *Catal. Today* **2002**, *76*, 235−246.
(32) Lei, Y. Z.; Zhao, G. H.; Liu, M. C.; Zhang, Z. N.; Tong, X. L.; Cao, T. C. *J. Phys. Chem. C* **2009**, *113*, 19067−19076.
(33) Ghicov, A.; Macak, J. M.; Tsuchiya, H.; Kunze, J.; Haeublein, V.; Frey, L.; Schmuki, P. *Nano Lett.* **2006**, *6*, 1080−1082.

(34) De Jongh, P. E.; Meulenkamp, E. A.; Vanmaekelbergh, D.; Kelly, J. J. *J. Phys. Chem. B* **2000**, *104*, 7686−7693.
(35) Jiang, Y. H.; Wu, M.; Wu, X. J.; Sun, Y. M.; Yin, H. B. *Mater. Lett.* **2009**, *63*, 275−278.
(36) Liu, Z.; Zhang, X.; Nishimoto, S.; Jin, M.; Tryk, D. A.; Murakami, T.; Fujishima, A. *J. Phys. Chem. C* **2008**, *112*, 253−259.
(37) Zhang, H.; Zong, R. L.; Zhu, Y. F. *J. Phys. Chem. C* **2009**, *113*, 4605−4611.
(38) Zheng, L. R.; Zheng, Y. H.; Chen, C. Q.; Zhan, Y. Y.; Lin, X. Y.; Zheng, Q.; Wei, K. M.; Zhu, J. F. *Inorg. Chem.* **2009**, *48*, 1819−1825.
(39) Wang, H. H.; Baek, S.; Lee, J.; Lim, S. *Chem. Eng. J.* **2009**, *146*, 355−361.
(40) Kontos, A. I.; Likodimos, V.; Stergiopoulos, T.; Tsoukleris, D. S.; Falaras, P.; Rabias, I.; Papavassiliou, G.; Kim, D.; Kunze, J.; Schmuki, P. *Chem. Mater.* **2009**, *21*, 662−672.
(41) Mohapatra, S. K.; Banerjee, S.; Misra, M. *Nanotechnology* **2008**, *19*, 315601−315607.
(42) Izumi, Y.; Itoi, T.; Peng, S.; Oka, K.; Shibata, Y. *J. Phys. Chem.C* **2009**, *113*, 6706−6718.
(43) Li, P. Q.; Zhao, G. H.; Cui, X.; Zhang, Y. G.; Tang, Y. T. *J. Phys. Chem. C* **2009**, *113*, 2375−2383.
(44) Kim, J. C.; Choi, J.; Lee, Y. B.; Hong, J. H.; Lee, J. I.; Yang, J. W.; Lee, W. I.; Hur, N. H. *Chem. Commun.* **2006**, *48*, 5024−5026.
(45) Xiao, F. X.; Wang, F. C.; Fu, X. Z.; Zheng, Y. *J. Mater. Chem.* **2012**, *22*, 2868−2877.
(46) Xiao, F. X. *J. Mater. Chem.* **2012**, *22*, 7819−7830.
(47) Xiao, F. X. *Chem. Commun.* **2012**, *48*, 6538−6540.
(48) Kostedt, W. L.; Ismail, A. A.; Mazyck, D. W. *Ind. Eng. Chem. Res.* **2008**, *47*, 1483−1487.
(49) Liao, D. L.; Badour, C. A.; Liao, B. Q. *J. Photochem. Photobiol. A* **2008**, *194*, 11−19.
(50) Yu, H. D.; Zhang, Z. P.; Han, M. Y.; Hao, X. T.; Zhu, F. R. *J. Am. Chem. Soc.* **2005**, *127*, 2378−2379.
(51) Yu, Q. J.; Fu, W. Y.; Yu, C. L.; Yang, H. B.; Wei, R. H.; Li, M. H.; Liu, S. K.; Sui, Y. M.; Liu, Z. L.; Yuan, M. X.; Zou, G. T.; Wang, G. R.; Shao, C. L.; Liu, Y. C. *J. Phys. Chem. C* **2007**, *111*, 17521−17526.
(52) Jiang, H. B.; Gao, L.; Zhang, Q. H. *J. Inorg. Mater.* **2003**, *18*, 695−698.
(53) Yang, S. G.; Quan, X.; Li, X. Y.; Liu, Y. Z.; Chen, S.; Chen, G. H. *Phys. Chem. Chem. Phys.* **2004**, *6*, 659−664.
(54) Zhang, Z. H.; Yuan, Y.; Fang, Y. J.; Liang, L. H.; Ding, H. C.; Jin, L. T. *Talanta* **2007**, *73*, 523.
(55) Chen, D.; Zhang, H.; Hu, S.; Li, J. H. *J. Phys. Chem. C* **2008**, *112*, 117−122.
(56) Zhang, Q.; Fan, W.; Gao, L. *Appl. Catal., B* **2007**, *76*, 168−173.
(57) Qiu, J.; Jin, Z.; Liu, Z.; Liu, X.; Liu, G.; Wu, W.; Zhang, X.; Gao, X. *Thin Solid Films* **2007**, *515*, 2897−2902.
(58) Qiu, J.; Yu, W.; Gao, X.; Li, X. *Nanotechnology* **2006**, *17*, 4695−4698.
(59) Thitima, R.; Takashi, S.; Susumu, Y. *Sol. Energy Mater. Sol. Cells* **2008**, *92*, 1445−1449.
(60) Kim, S. S.; Na, S. In.; Nah, Y. C. *Electrochim. Acta* **2011**, *58*, 503−509.
(61) Benkara, S.; Zerkout, S. *J. Mater. Environ. Sci.* **2010**, *1*, 183−188.
(62) Zhang, Z. H.; Yuan, Y.; Liang, L. H.; Cheng, Y. X.; Shi, G. Y.; Jin, L. T. *J. Hazard. Mater.* **2008**, *158*, 517−522.
(63) Yang, H. Y.; Yu, S. F.; Lau, S. P.; Zhang, X. W.; Sun, D. D.; Jun, G. *Small* **2009**, *5*, 2260−2264.
(64) Wang, D. A.; Liu, Y.; Wang, C. W.; Zhou, F.; Liu, W. M. *ACS Nano* **2009**, *3*, 1249−1257.
(65) Shin, Y.; Lee, S. *Nano Lett.* **2008**, *8*, 3171−3173.
(66) Liu, Z. Y.; Zhang, X. T.; Nishimoto, S.; Jin, M.; Tryk, D. A.; Murakami, T.; Fujishima, A. *J. Phys. Chem. C* **2008**, *112*, 253−259.
(67) Liu, Z. Y.; Zhang, X. T.; Nishimoto, S.; Murakami, T.; Fujishima, A. *Environ. Sci. Technol.* **2008**, *42*, 8547−8551.
(68) Lindstrom, H.; Holmberg, A.; Magnusson, E.; Lindquist, S. E.; Malmqvist, L.; Hagfeldt, A. *Nano Lett.* **2001**, *1*, 97−100.
(69) Lindstrom, H.; Holmberg, A.; Magnusson, E.; Lindquist, S. E.; Malmqvist, L.; Hagfeldt, A. *J. Photochem. Photobiol., A* **2001**, *145*, 107−112.
(70) Zeng, H. C.; Xie, F.; Wong, K. C.; Mitchell, K. A. R. *Chem. Mater.* **2002**, *14*, 1788−1796.
(71) Wei, X. M.; Zeng, H. C. *Chem. Mater.* **2003**, *15*, 433−442.
(72) Barr, T. L.; Seal, S. *J. Vac. Sci. Technol., A* **1995**, *13*, 1239−1246.
(73) Biniak, S.; Szymanski, G.; Siedlewski, J.; Swiatkowski, A. *Carbon* **1997**, *35*, 1799−1810.
(74) Dou, J.; Zeng, H. C. *J. Phys. Chem. C* **2012**, *116*, 7767−7775.
(75) Centeno, M. A.; Paulis, M.; Montes, M.; Odriozola, J. A. *Appl. Catal., B* **2005**, *61*, 177−183.
(76) Li, J.; Tang, S. B.; Lu, L.; Zeng, H. C. *J. Am. Chem. Soc.* **2007**, *129*, 9401−9409.
(77) Li, J.; Zeng, H. C. *Chem. Mater.* **2006**, *18*, 4270−4277.
(78) Micic, O. I.; Nenadovic, M. T.; Peterson, M. W.; Nozik, A. J. *J. Phys. Chem.* **1987**, *91*, 1295−1297.
(79) Pian, X. T.; Lin, B. Z.; Chen, Y. L.; Kuang, J. D.; Zhang, K. Z.; Fu, L. M. *J. Phys. Chem. C* **2011**, *115*, 6531−6539.
(80) Yao, K. X.; Zeng, H. C. *J. Phys. Chem. C* **2007**, *111*, 13301−13308.
(81) Yang, Y.; Wang, X. H.; Sun, C. K.; Li, L. T. *J. Appl. Phys.* **2009**, *105*, 094304−094309.
(82) He, J.; Mosurkal, R.; Samuelson, L. A.; Li, L.; Kumar, J. *Langmuir* **2003**, *19*, 2169−2174.
(83) Kumar, P. M.; Badrinarayanan, S.; Sastry, M. *Thin Solid Films* **2000**, *358*, 122−130.
(84) Georgekutty, R.; Seery, M. K.; Pillai, S. C. *J. Phys. Chem. C* **2008**, *112*, 13563−13570.
(85) Xu, Y. -J.; Zhuang, Y.; Fu, X. Z. *J. Phys. Chem. C* **2010**, *114*, 2669−2676.
(86) Zhang, Y. H.; Tang, Z. R.; Fu, X. Z.; Xu, Y. J. *ACS Nano* **2011**, *5*, 7426−7435.
(87) Serpone, N.; Maruthamuthu, P.; Pichat, P.; Pelizzetti, E.; Hidaka, H. *J. Photochem. Photobiol., A* **1995**, *85*, 247−255.
(88) Spathis, P.; Poulios, I. *Corros. Sci.* **1995**, *37*, 673−680.
(89) Zheng, L. R.; Zheng, Y. H.; Chen, C. Q. *Inorg. Chem.* **2009**, *48*, 1819−1852.